Available online at www.sciencedirect.com
ScienceDirect
International Journal of Heat and Mass Transfer 51 (2008) 1946–1954
International Journal of HEAT and MASS TRANSFER
www.elsevier.com/locate/ijhmt

Magnetoconvection in an enclosure with partially active vertical walls

P. Kandaswamy *, S. Malliga Sundari, N. Nithyadevi

UGC-DRS Centre for Fluid Dynamics, Department of Mathematics, Bharathiar University, Coimbatore 641 046, India

Received 22 March 2007; received in revised form 8 June 2007
Available online 14 August 2007

Abstract

Magnetoconvection of an electrically conducting fluid in a square cavity with partially thermally active vertical walls is investigated numerically. The active part of the left side wall is at a higher temperature than the active part of the right side wall. The top, bottom and the inactive parts of the side walls are thermally inactive. Nine different combinations of the relative positions of the active zones are considered. The governing equations are discretized by the control volume method with QUICK scheme and solved numerically by SIMPLE algorithm for the pressure–velocity coupling together with underrelaxation technique. The results are obtained for Grashof numbers between 10^4 and 10^6, Hartmann numbers between 0 and 100 and Prandtl numbers 0.054–2.05. The heat transfer characteristics are presented in the form of streamlines and isotherms. The heat transfer rate is maximum for the middle–middle thermally active locations while it is poor for the top–bottom thermally active locations. The average Nusselt number decreases with an increase of Hartmann number and increases with an increase of Grashof number. For sufficiently large magnetic field $Ha = 100$ the convective mode of heat transfer is converted into conductive mode in the low region of Grashof number than in the high region.

Keywords: Magnetoconvection; Partially active walls; Square cavity; Control volume method

1. Introduction

Magnetoconvection occurs under many circumstances and received a great deal of attention as it finds applications in geophysics, astrophysics, aerodynamics, engineering and industries. Magnetoconvection in cavities particularly has applications in solar technologies, safety aspects of gas cooled reactors, crystal growth in liquids, material manufacturing technology and haemodialysis. There are situations where heat is being generated during certain operations and may be detrimental to the equipment. The undesirable amount of heat is to be removed as far as possible. For instance gas turbine blades, walls of an I. C. engine combustion chamber, outer surface of a space vehicle, all depend on their durability on rapid heat removal from their surfaces. Natural convection in a rectangular cavity with differentially heated side walls and insulated horizontal surfaces has been the subject of great interest.

Davis [3] studied the two-dimensional natural convection in a square cavity with differentially heated side walls and has suggested a bench mark solution. Valencia and Frederick [15] investigated the natural convection of air in square cavities with half-active and half-insulated vertical walls numerically for various Rayleigh numbers. They observed that the heat transfer rates could be controlled to a certain extent by varying the relative positions of the hot and cold elements. Ostrach [10] has demonstrated natural convection problems in science and technology. The complexities of the phenomena has also been discussed. Rudraiah et al. [12,13] studied numerically the effect of magnetic field on the flow driven by the combined mechanism of buoyancy and thermocapillarity in a rectangular open cavity filled with low Prandtl number fluid and observed that as the strength of the magnetic field increases, the buoyancy-driven convection decreases.

Kandaswamy and Kumar [7] studied the natural convection of water near its density maximum in the presence

* Corresponding author. Tel.: +91 422 2426764; fax: +91 422 2422387.
E-mail address: pgkswamy@yahoo.co.in (P. Kandaswamy).

0017-9310/$ - see front matter © 2007 Elsevier Ltd. All rights reserved.
doi:10.1016/j.ijheatmasstransfer.2007.06.025

Nomenclature

B_0	magnetic field
g	acceleration due to gravity
Gr	Grashof number
Ha	Hartmann number
L	length of the cavity
Nu	local Nusselt number
$\overline{Nu}$	average Nusselt number
p	pressure
Pr	Prandtl number
t	dimensional time
T	dimensionless temperature
u, v	velocity components
U, V	dimensionless velocity components
x, y	dimensional coordinates
X, Y	dimensionless coordinates

Greek symbols

α	thermal diffusivity
β	coefficient of thermal expansion
μ	dynamic viscosity
ν	kinematic viscosity
θ	temperature
ρ	density
σ_e	electrical conductivity of the medium
τ	dimensionless time

Subscripts

c	cold wall
h	hot wall
o	reference state

of uniform magnetic field. They observed that the effect of the magnetic field on the natural convection is to inhibit the heat transfer rate. Bethancourt et al. [2] made numerical computations of natural convection in a side-heated square cavity with two layers of immiscible Boussinesque liquids. They found the impacts of a deformable interface and of surface tension in local behaviour of heat transfer characteristics. Aydin et al. [1] performed a numerical study of steady natural convection of air in two-dimensional enclosure isothermally heated from one side and cooled from the ceiling. They found the effect of heat transfer rate to be more significant when the enclosure is shallow and the influence of aspect ratio is stronger when the enclosure is tall and the Rayleigh number is high.

Saravanan and Kandaswamy [14] analysed the convection in a low Prandtl number fluid driven by the combined mechanism of buoyancy and surface tension in the presence of a uniform vertical magnetic field. It has been shown that the heat transfer across the cavity from the hot wall to cold wall becomes poor for a decrease in thermal conductivity in the presence of vertical magnetic field. Frederick and Quiroz [5] have remarked that the transition to convection occurs in the range of Rayleigh numbers from 10^3 to 10^5 in their study on the transition from conduction to convection regime in a cubical enclosure with a partially heated wall. Deng et al. [4] numerically studied a two-dimensional, steady and laminar natural convection in a rectangular enclosure with discrete heat sources on walls. They have remarked that the heat source on the floor increases the thermal instability and acts as a proportional effect on convection, while the heat source on the side wall increases the thermal stability and acts as a reverse effect on convection.

Nithyadevi et al. [8] investigated the effect of aspect ratio on the natural convection of a fluid contained in a rectangular cavity with partially thermally active side walls. They found that heat transfer rate increases with increase in the aspect ratio and when the cooling location is at the top of the enclosure. Nithyadevi et al. [9] further investigated the transient natural convection in a square cavity with partially thermally active side walls. The thermally active regions were considered to be periodic in time. The results were obtained for various values of amplitude, period and Grashof numbers and different thermally active locations. They observed the heat transfer to increase for periods 1 and 5 and to decrease for period 3 and the average Nusselt number to behave nonlinearly as a function of period.

The present study deals with the natural convection in a square cavity filled with an electrically conducting fluid with partially thermally active vertical walls, for nine different combinations of active locations in the presence of external magnetic field parallel to gravity. The hot region is located at the top, middle and bottom and the cold region is moved from bottom to top, to locate the positions where the heat transfer rate is maximum and minimum. The results are displayed graphically in the form of streamlines and isotherms, which show the effect of magnetic field with different heating locations of the side walls.

2. Mathematical formulation

Consider the unsteady two-dimensional natural convection flow of fluid in a square cavity of length L as shown in Fig. 1. The partially thermally active side walls of the cavity are maintained at two different but uniform temperatures, namely, θ_h and θ_c with $\theta_h > \theta_c$, respectively. The remaining boundaries of the cavity are thermally insulated. Nine different cases are studied (viz) the hot location is moving from top to bottom of the left wall and the cold location moving from bottom to top of the right wall. The gravity acts normal to the x-axis and the external magnetic field B_0 is applied parallel to gravity. It is assumed that the induced magnetic field is negligible compared to the applied magnetic field. Under the above assumptions, the

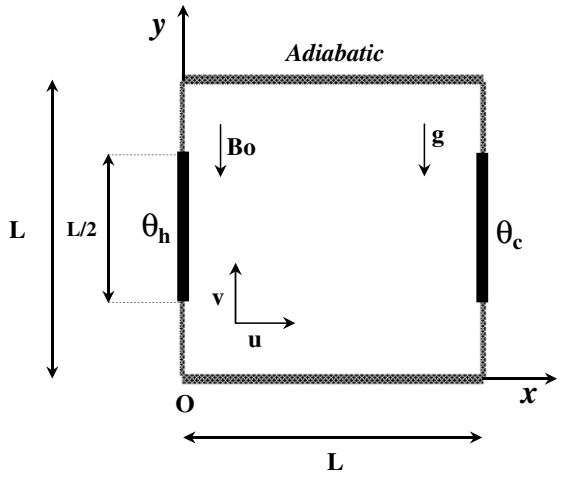

Fig. 1. Physical configuration.

conservation equations of mass, momentum and energy in a two-dimensional Cartesian co-ordinate system are

$$\frac{\partial u}{\partial x}+\frac{\partial v}{\partial y}=0 \tag{1}$$

$$\frac{\partial u}{\partial t}+u\frac{\partial u}{\partial x}+v\frac{\partial u}{\partial y}=-\frac{1}{\rho_0}\frac{\partial p}{\partial x}+\nu\nabla^2 u-\frac{\sigma_e B_0^2}{\rho_0}u \tag{2}$$

$$\frac{\partial v}{\partial t}+u\frac{\partial v}{\partial x}+v\frac{\partial v}{\partial y}=-\frac{1}{\rho_0}\frac{\partial p}{\partial y}+\nu\nabla^2 v-\frac{\rho}{\rho_0}g \tag{3}$$

$$\frac{\partial \theta}{\partial t}+u\frac{\partial \theta}{\partial x}+v\frac{\partial \theta}{\partial y}=\alpha\nabla^2\theta \tag{4}$$

where

$$\rho=\rho_0[1-\beta(\theta-\theta_c)]$$

The appropriate initial and boundary conditions are:

$$\begin{aligned}
&t=0: \quad u=v=0, \quad \theta=\theta_c, \quad 0\leqslant x\leqslant L, \quad 0\leqslant y\leqslant L\\
&t>0: \quad u=v=0, \quad \tfrac{\partial\theta}{\partial y}=0, \quad y=0\&L\\
&\theta=\theta_h, \quad \text{active part}, \quad \tfrac{\partial\theta}{\partial x}=0, \quad x=0\\
&\theta=\theta_c, \quad \text{active part}, \quad \tfrac{\partial\theta}{\partial x}=0, \quad x=L
\end{aligned}$$

Introducing the following nondimensional variables:

$$\tau=\frac{t}{L^2/\nu}, \quad (X,Y)=\frac{(x,y)}{L}, \quad (U,V)=\frac{(u,v)}{\nu/L},$$

$$T=\frac{\theta-\theta_c}{\theta_h-\theta_c}, \quad \text{with } \theta_h>\theta_c$$

The nondimensional form of Eqs. (1)–(4) are obtained as

$$\frac{\partial U}{\partial X}+\frac{\partial V}{\partial Y}=0 \tag{5}$$

$$\frac{\partial U}{\partial \tau}+U\frac{\partial U}{\partial X}+V\frac{\partial U}{\partial Y}=-\frac{\partial P}{\partial X}+\nabla^2 U-Ha^2U \tag{6}$$

$$\frac{\partial V}{\partial \tau}+U\frac{\partial V}{\partial X}+V\frac{\partial V}{\partial Y}=-\frac{\partial P}{\partial Y}+\nabla^2 V+GrT \tag{7}$$

$$\frac{\partial T}{\partial \tau}+U\frac{\partial T}{\partial X}+V\frac{\partial T}{\partial Y}=\frac{1}{Pr}\nabla^2 T \tag{8}$$

The initial and boundary conditions in the dimensionless form are:

$$\begin{aligned}
&\tau=0: \quad U=V=0, \quad T=0, \quad 0\leqslant X\leqslant 1, \quad 0\leqslant Y\leqslant 1,\\
&\tau>0: \quad U=V=0, \quad \tfrac{\partial T}{\partial Y}=0, \quad \text{at } =Y=0 \text{ and } 1,\\
&T=1, \quad \text{active part} \quad \tfrac{\partial T}{\partial X}=0, \quad X=0,\\
&T=0, \quad \text{active part} \quad \tfrac{\partial T}{\partial X}=0, \quad X=1.
\end{aligned}$$

The nondimensional parameters that appear in the equations are, $Gr=\frac{g\beta(\theta_h-\theta_c)L^3}{\nu^2}$ Grashof number, $Ha^2=\frac{B_o^2L^2\sigma_e}{\mu}$ Hartmann number and $Pr=\frac{\nu}{\alpha}$ Prandtl number. The local Nusselt number is defined by $Nu=\frac{\partial T}{\partial X}|_{\,y=0}$ resulting in the average Nusselt number as $\overline{Nu}=\frac{1}{h}\int_h Nu\,dY$, | where $h=\frac{L}{2}$ is height of heating location.

3. Method of solution

The governing equations (5)–(8) are discretized by control volume method and the coupling between velocity and pressure is solved by SIMPLE algorithm Patankar [11]. The discretized form of the Eq. (6) can be written as

$$\begin{aligned}
&\frac{\phi_P-\phi_P^0}{\Delta\tau}\Delta V+[(U\phi)_e-(U\phi)_w]\Delta Y+[(V\phi)_n-(V\phi)_s]\Delta X\\
&\quad=\Gamma^\phi\left[\left(\frac{\partial\phi}{\partial X}\right)_e-\left(\frac{\partial\phi}{\partial X}\right)_w\right]\Delta Y\\
&\qquad+\Gamma^\phi\left[\left(\frac{\partial\phi}{\partial Y}\right)_n-\left(\frac{\partial\phi}{\partial Y}\right)_s\right]\Delta X+S^\phi(X,Y)
\end{aligned} \tag{9}$$

The third order accurate deferred QUICK scheme of Hayase et al. [6] is employed to minimize the numerical diffusion for the convective terms to the discretized Eq. (9) to obtain the form

$$\begin{aligned}
a_P\phi_P^n=\;&a_E\phi_E^n+a_W\phi_W^n+a_N\phi_N^n+a_S\phi_S^n+b_E\phi_E^{n-1}+b_W\phi_W^{n-1}\\
&+b_N\phi_N^{n-1}+b_S\phi_S^{n-1}+b_{EE}\phi_{EE}^{n-1}+b_{WW}\phi_{WW}^{n-1}+b_{NN}\phi_{NN}^{n-1}\\
&+b_{SS}\phi_{SS}^{n-1}+b_p\phi_p^{n-1}+S^\phi(X,Y)
\end{aligned}$$

where

$$a_E=D_e+[|0,-F_e|], a_W=D_w+[|0,F_w|]$$

$$a_N=D_n+[|0,-F_n|], \; a_S=D_s+[|0,F_s|]$$

$$a_P=a_E+a_W+a_N+a_S+a_P^0$$

$$b_E=\frac{1}{8}\{-3[|0,F_e|]-2[|0,-F_e|]+[|0,-F_w|]\}$$

$$b_W=\frac{1}{8}\{-3[|0,-F_w|]-2[|0,F_w|]+[|0,F_e|]\}$$

$$b_N=\frac{1}{8}\{-3[|0,F_n|]-2[|0,-F_n|]+[|0,-F_s|]\}$$

$$b_S=\frac{1}{8}\{-3[|0,-F_s|]-2[|0,F_s|]+[|0,F_n|]\}$$

$$b_{EE}=\frac{-1}{8}[|0,-F_e|], b_{WW}=\frac{-1}{8}[|0,F_w|]$$

$$b_{NN}=\frac{-1}{8}[|0,-F_n|], b_{SS}=\frac{-1}{8}[|0,F_s|]$$

$$b_P=b_E+b_W+b_N+b_S+b_{EE}+b_{WW}+b_{NN}+b_{SS}+a_P^0$$

Table 1
Comparison of average Nusselt numbers for different Grashof numbers and Hartmann numbers

Gr	Ha	$\overline{Nu}$	
		Rudraiah et al. [12]	Present
2×10^4	0	2.5188	2.6237
	10	2.2234	2.3234
	50	1.0856	1.0987
	100	1.0110	1.0245
2×10^5	0	4.9198	5.1876
	10	4.8053	4.9825
	50	2.8442	2.9784
	100	1.4317	1.6318
2×10^6	0	8.7030	8.9341
	10	8.6463	8.7936
	50	7.5825	7.6153
	100	5.5415	5.5918

The resulting set of discretized equations for each variable are solved by a line-by-line procedure, combining the tri-diagonal matrix algorithm (TDMA). Under relaxation technique is employed for the pressure correction. The mass balance for global convergence is taken as 10^{-7}.

Uniform staggered grid system is employed in the present study. It is found that the grid 51×51 is sufficiently fine to ensure a grid independent solution. Accuracy of the numerical procedure is first validated by the comparison between the predicted results with the bench mark solutions of Davis [3]. The results are found to be in good agreement with the benchmark solution. The present numerical results are compared with those of Rudraiah et al. [12] in Table 1 and found that the control volume method with SIMPLE algorithm is fast converging.

4. Results and discussion

The effect of magnetic field on the buoyancy-driven convection of an electrically conducting fluid in a square cavity, with partially thermally active side walls is investigated numerically. The computations are carried out for Grashof numbers from 10^4 to 10^6, Hartmann numbers from 0 to 100 and Prandtl numbers from 0.054 to 2.05 and $Pr = 0.71$ is considered for all other computations. The flow fields and the temperature gradients inside the cavity are presented to illustrate the impact of the magnetic field and positioning of the active locations on the heat transfer characteristics. The heated location is always kept on the left wall and the cooled location on the right wall.

4.1. Effect due to change in active locations

Figs. 2a–i and 3a–i show the streamlines and isotherms for the nine different combinations of active locations for a magnetic field with $Ha = 10$ and $Gr = 10^5$. In the case of top–bottom position, two fully developed clockwise rotating vortices are seen inside a large cell in Fig. 2a. The buoyancy force which ascend the fluid particles heated near the hot wall acts parallel to the hot wall and moves horizontally and descends towards the cold location. Fig. 3a shows that the corresponding isotherms are almost parallel to the horizontal wall at the center of the cavity as the flow is stagnant at the core.

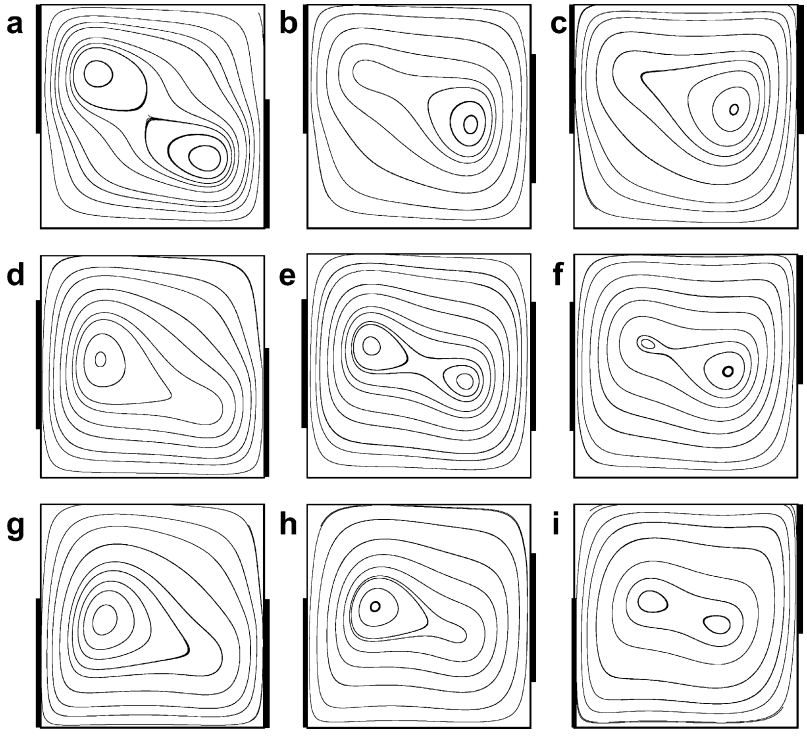

Fig. 2. (a–i) Steady state streamlines for nine different locations, $Pr = 0.71$, $Ha = 10$ and $Gr = 10^5$.

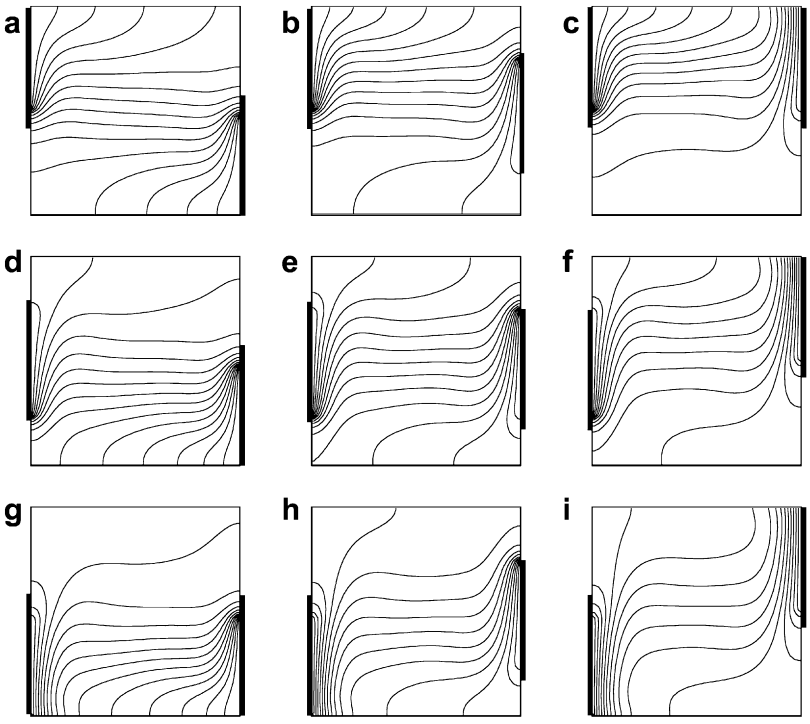

Fig. 3. (a–i) Steady state isotherms for nine different locations, $Pr = 0.71$, $Ha = 10$ and $Gr = 10^5$.

Fig. 2b shows the streamlines for the top–middle active case. One of the small vortices disappears to form single enlarged cell which moves towards the cold region, the corresponding isotherms in Fig. 3b indicate that the convective heat transfer is less at the bottom of the cavity. In the top-top active position, and the bottom–bottom active position indicate a mirror image effect with flow concentration at the active regions as seen from Fig. 2c and g. The corresponding isotherms in Fig. 3c and g reveals the convective mode of heat transfer in the active regions and the bottom and top of the enclosure are thermally inactive.

In the middle–bottom active position in Fig. 2d a single clockwise rotating cell exists near the hot location and elongates towards the cold region. In Fig. 3d the isotherms indicate that the hot particles transport the energy by convection which is meager at the top of the cavity. Fig. 2e shows the streamlines for the middle–middle active position. Two small convective cells are formed in the core with a larger cell around them with flow all over the cavity. The corresponding isotherms in Fig. 3e indicates that the convective mode of heat transfer prevails all over the cavity except at the center. In the middle–top case in Fig. 2f one of the inner vortices shrinks completely within the larger cell. The isotherms for the above flow in Fig. 3f show the formation of thermal boundary layer near the active regions.

In the bottom–middle active case in Fig. 2h the single enlarged cell exists and the flow is improved to all parts of the cavity. Fig. 3h indicates that the isotherms are more concentrated near the active zones with the formation of the thermal boundary layers and the energy is transported through moderate convection. In the bottom–top active location the single larger cell is horizontally elongated with two tiny vortices inside in Fig. 2i is observed. The formation of the thermal boundary layer near the active zones which reduce the flow and temperature gradient at the core region as clearly seen in Fig. 3i.

4.2. Effect of increase in external magnetic field strength

In Figs. 4–6a–c the streamlines and isotherms are depicted for top–bottom, middle–middle and bottom–top active positions with increasing magnetic fields with $Ha = 10$, 50 and 100. The impacts due to change in active locations and increase in the value of Hartmann number are depicted. In the streamline pattern the presence of two cells near the active zones gradually move to the center and decrease in size. The buoyancy force is reduced considerably. The intensities in the flow decreases owing to the increase in the magnetic field. This is expected since presence of magnetic field usually retards the flow which is observed from Table 2. The corresponding effect of the increase in magnetic field on the isotherms is that they are more straighten out since the magnetic field resists the flow and the convection is totally suppressed inside the cavity. As the Hartmann number increases, the temperature stratification in the core diminishes and the thermal boundary layer at the two active side walls disappear, Fig. 4–6c. Also the streamlines are elongated and the core region becomes broadly stagnated.

This effect is also seen in Fig. 13 in which the mid-height velocity profiles are flattened for higher values of

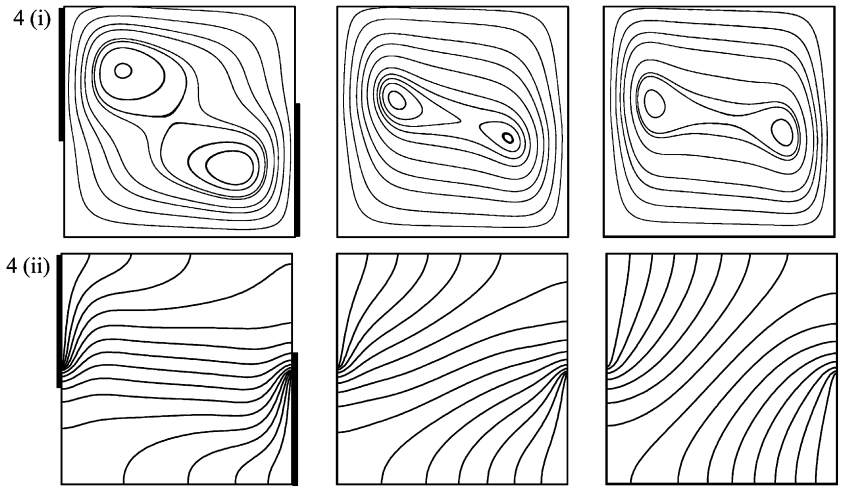

Fig. 4. (i)–(ii) Steady state streamlines and isotherms for $Pr = 0.71$, $Gr = 10^5$, (a) $Ha = 10$.

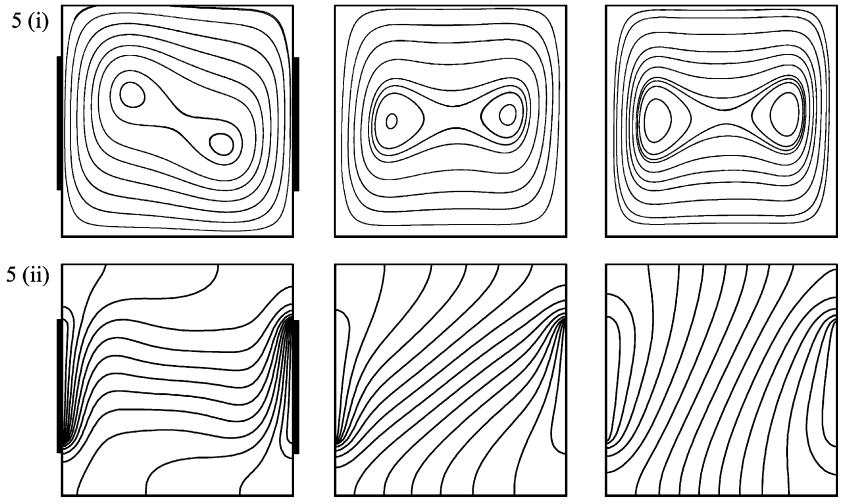

Fig. 5. (i)–(ii) Steady state streamlines and isotherms for $Pr = 0.71$, $Gr = 10^5$, (b) $Ha = 50$.

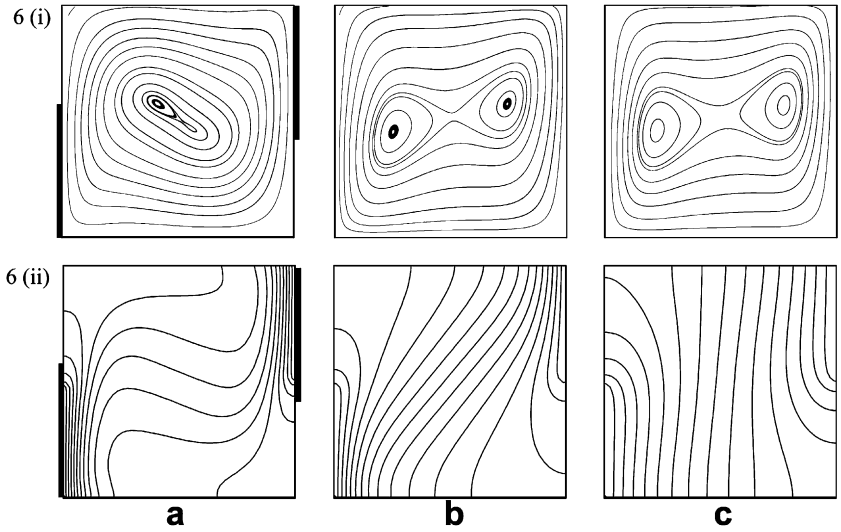

Fig. 6. (i)–(ii) Steady state streamlines and isotherms for $Pr = 0.71$, $Gr = 10^5$, (c) $Ha = 100$.

Table 2
Effect of Grashof number and Hartmann number on average Nusselt number, horizontal and vertical velocities for top–bottom active location

Gr	*Ha*	U_{max}	V_{max}	Avg. *Nu*
10^4	0	8.42	9.15	1.921038
	10	6.22	7.01	1.713625
	50	1.17	1.59	1.339501
	100	0.33	0.63	1.326234
10^5	0	20.06	27.65	2.989092
	10	17.77	26.03	2.877136
	50	6.48	12.55	1.817992
	100	2.80	5.86	1.421136
10^6	0	46.74	80.54	4.107253
	10	42.88	79.28	4.108758
	50	22.57	74.73	3.695692
	100	11.49	49.60	2.743037

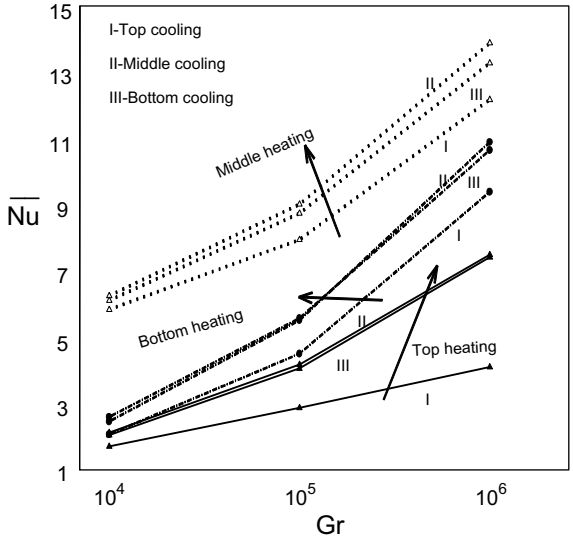

Fig. 7. Average *Nu* vs *Gr* for different locations, $Pr = 0.71$ and $Ha = 10$.

the Hartmann number $Ha = 50, 100$ which is shown for the bottom–top active case. The average Nusselt number for the different active locations are shown in Fig. 7 for various Grashof numbers. As expected when the Grashof number increases the average Nusselt number also increases, but the heat transfer rate is high in the middle–middle active locations and low for top–bottom active locations.

Fig. 8 shows the behaviour of the average Nusselt number, for different magnetic field strengths. In all the cases,

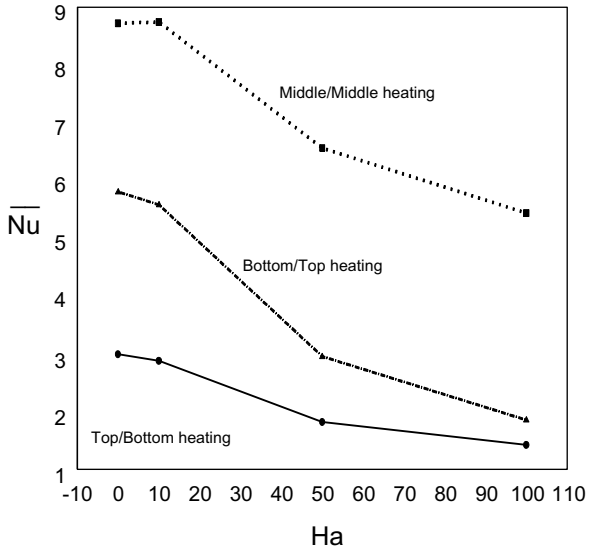

Fig. 8. Average *Nu* vs *Ha* for different locations, $Pr = 0.71$ and $Gr = 10^5$.

the heat transfer rate decreases as the Hartmann number increases. The average Nusselt number is very low in the top–bottom heating locations in comparison to all other cases. Also the velocities shown in Table 2 indicate that the heat transfer will be of almost conductive type beyond $Ha = 100$.

4.3. Time history of the transient state

Figs. 9 and 10 illustrates the transient results of streamlines and isotherms for the bottom–top active positions, for $Ha = 10$ and $Gr = 10^5$. In the beginning a small amount of fluid near the heating location is activated. For $\tau = 0.002$ a small clockwise rotating hot cell appears near the bottom heating location and the isotherms are almost parallel lines. They indicate conduction mode of heat transfer. At time $\tau = 0.008$ and 0.016 the clockwise rotating cell grows in size, moves slightly away from the boundary and expands while the isotherms become parabolic and spreads to half of the enclosure. At time $\tau = 0.032$ and 0.064 the convective cell has moved to the center, elongated to an elliptic shape and occupies the entire enclosure. The corresponding isotherms have reached the right side top cooling location and the thermal boundary layers are seen at the active locations and they are horizontal at the core indicating that convection has set inside the enclosure. At time $\tau = 1.024$

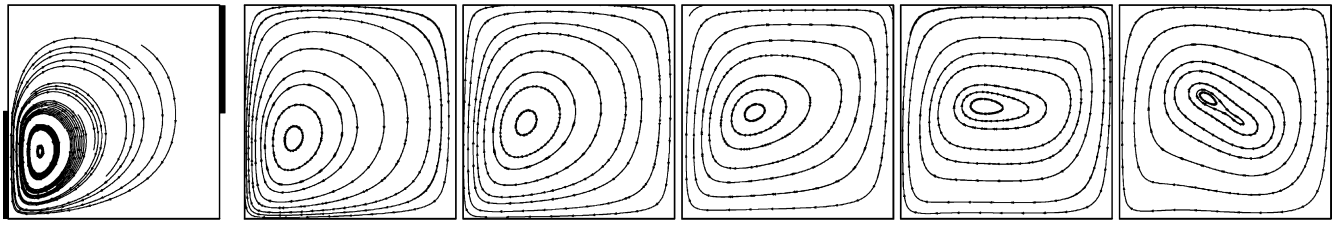

Fig. 9. Time history of streamlines for bottom–top heating locations, $Pr = 0.71$, $Ha = 10$ and $Gr = 10^5$.

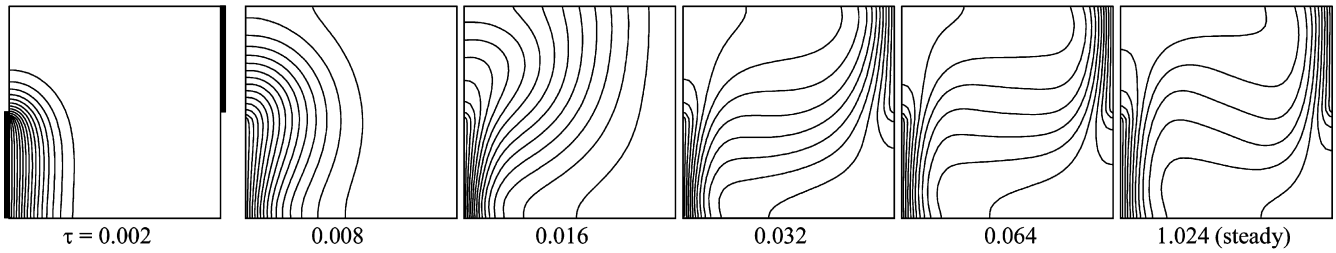

Fig. 10. Time history of isotherms for bottom-top heating locations, Pr = 0.71, $Ha = 10$ and $Gr = 10^5$.

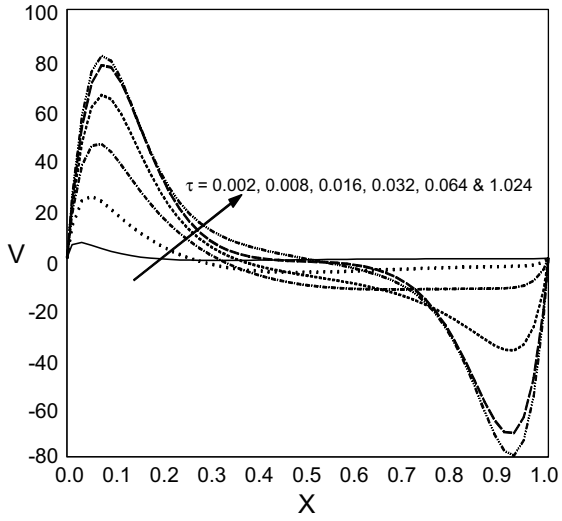

Fig. 11. Time history of mid-height velocity profile for bottom–top heating locations, $Pr = 0.71$, $Ha = 10$ and $Gr = 10^5$.

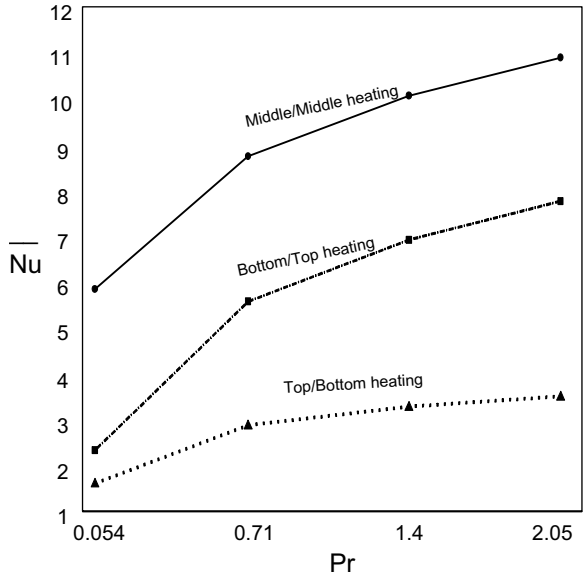

Fig. 12. Average Nusselt number vs Pr for different heating location, $Ha = 10$ and $Gr = 10^5$.

the streamline are tilted and the isotherms are further skewed depicting the steady state behaviour.

Fig. 11 exhibits the time history of the mid-height velocity profiles for the transient state for the bottom–top active positions, for $Ha = 10$ and $Gr = 10^5$. Initially the velocity increases only near the heating location and for further increase in time the velocity of the fluid particles near the cold location also increase and when the steady state is reached where the velocity curves coincide.

4.4. Effect of increase in Prandtl number

The increase in the average Nusselt number for the increase in the Prandtl number are shown in Fig. 12 for different heating locations, for $Ha = 10$ and $Gr = 10^5$. The rate of increase is high in the range for $Pr = 0.054$–0.71. It is also observed that in the middle–middle active location the heat transfer is more than in the other cases.

4.5. Time history of the steady state

The steady state variations in average Nusselt number with respect to time are shown in Fig. 14, for the bottom–top active positions, $Gr = 10^5$ and for different mag-

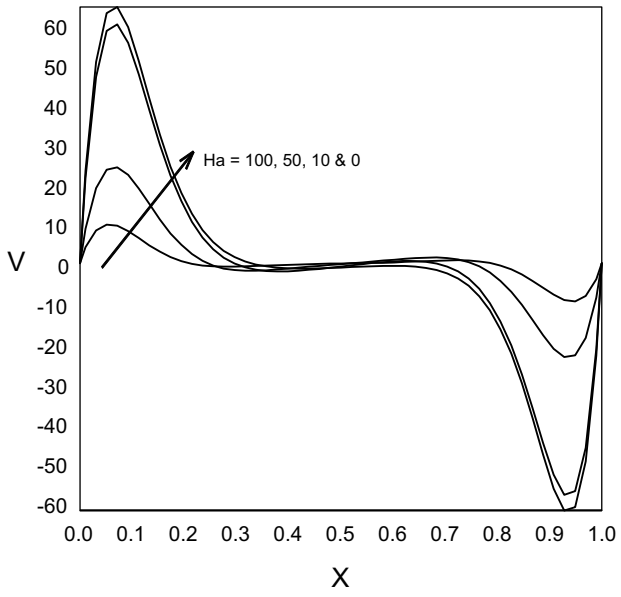

Fig. 13. Mid-height velocity profiles for bottom–top active location, $Pr = 0.71$ and $Gr = 10^5$.

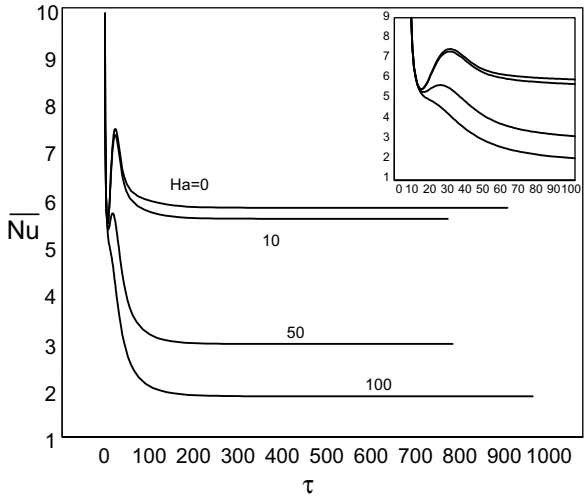

Fig. 14. Average Nu vs time for bottom–top active location, $Pr = 0.71$ and $Gr = 10^5$.

netic field strengths. The rate of heat transfer is minimum when $Ha = 100$. The inner figure shows early stages of the flow development. During the transition from conduction to convection mode the average Nusselt number curve attains a minimum, then increases before reaching the steady state for low magnetic fields. As the magnetic field strength is increased to 100 it reaches the minimum and attains the steady state.

5. Conclusion

Natural convection in a square cavity with partially thermally active vertical walls in the presence of magnetic field is studied numerically with nine different combination of the active positions. It is found that the heat transfer rate is enhanced in the middle–middle thermally active locations while it is poor for the top–bottom case. The average Nusselt number increases with increase in Grashof number but decreases with increase in Hartmann number. As strength of the magnetic field is increased ($Ha = 100$) convection is completely suppressed and the heat transfer in the cavity is mostly due to conduction mode. The rate of flow also decreases for increase in Hartmann number in all different active positions. Increase in Prandtl number leads to increase in the average Nusselt number.

References

[1] O. Aydin, A. Unal, T. Ayhan, Natural convection in rectangular enclosures heated from one side and cooled from the ceiling, Int. J. Heat Mass Transfer 42 (1999) 2345–2355.
[2] L. Bethancourt, M. Hashiguchi, K. Kuwahara, J.M. Hyun, Natural convection of a two-layer fluid in a side-heated cavity, Int. J. Heat Mass Transfer 42 (1999) 2427–2437.
[3] G. Davis, Natural convection of air in a square cavity: a bench mark numerical solution, Int. J. Numer. Methods Fluids 3 (1983) 249–264.
[4] Q. Deng, G. Tang, Y. Li, A combined temperature scale for analyzing natural convection in rectangular enclosures with discrete wall heat sources, Int. J. Heat Mass Transfer 45 (2002) 3437–3446.
[5] R.L. Frederick, F. Quiroz, On transition from conduction to convection regime in a cubical enclosure with a partially heated wall, Int. J. Heat Mass Transfer 44 (2001) 1699–1709.
[6] T. Hayes, J.A.C. Humphrey, R. Greif, A consistently formulated QUICK scheme for fast and stable convergence using finite volume iterative calculation procedures, J. Comput. Phys. 98 (1992) 108–118.
[7] P. Kandaswamy, K. Kumar, Buoyancy-driven nonlinear convection in a square cavity in the presence of a magnetic field, Acta Mech. 136 (1999) 29–39.
[8] N. Nithyadevi, P. Kandaswamy, J. Lee, Natural convection in a rectangular cavity with partially active side walls, Int. J. Heat Mass Transfer 50 (2007) 942–948.
[9] N. Niyhyadevi, P. Kandaswamy, S. Sivasankaran, Natural convection on a square cavity with partially active vertical walls: time periodic boundary condition, Math. Probl. Eng. 2006 (2006) 1–16.
[10] S. Ostrach, Natural convection in enclosures, J. Heat Transfer 110 (1988) 1175–1190.
[11] S.V. Patankar, Numerical Heat Transfer and Fluid Flow, Hemisphere, McGraw-Hill, Washington, DC, 1980.
[12] N. Rudraiah, R.M. Barron, M. Venkatachalappa, C.K. Subbaraya, Effect of a magnetic field on free convection in a rectangular enclosure, Int. J. Eng. Sci. 33 (1995) 1075–1084.
[13] N. Rudraiah, M. Venkatachalappa, C.K. Subbaraya, Combined surface tension and buoyancy-driven convection in a rectangular open cavity in the presence of a magnetic field, Int. J. Non-Linear Mech. 30 (1995) 759–770.
[14] S. Saravanan, P. Kandaswamy, Low Prandtl number magnoconvection in cavities: effect of variable thermal conductivity, Z. Angew. Math. Mech. 80 (2000) 570–576.
[15] A. Valencia, R.L. Frederick, Heat transfer in square cavities with partially active vertical walls, Int. J. Heat Mass Transfer 32 (1989) 1567–1574.